

## Materials and methods

### Mice and embryos

C57BL/6 mice were purchased from Japan SLC (Hamamatsu, Japan) and *Notch1* mutant mice<sup>13</sup> were from Jackson Laboratory (Bar Harbor, ME). To generate embryos, timed matings were set up between *Notch1*<sup>+/−</sup> mice. The time at midday (12 PM) was taken to be E0.5 for the plugged mice.

### In vitro P-Sp culture

P-Sp culture was performed as described previously.<sup>14</sup> In brief, isolated P-Sp regions of E9.5 embryos were dissociated by incubation with 250 protease units (PU)/mL dispase (Godo Shusei, Tokyo, Japan) for 20 minutes and cell-dissociation buffer (Gibco BRL, Carlsbad, CA) for 20 minutes at 37°C, followed by vigorous pipetting. Approximately  $5 \times 10^4$  P-Sp-derived cells were suspended in 300  $\mu$ L of serum-free StemPro media (Life Technologies, Gaithersburg, MD) supplemented with 50 ng/mL stem-cell factor (SCF), 5 ng/mL interleukin-3 (IL3; gifts from Kirin Brewery, Takasaki, Japan), and 10 ng/mL mouse oncostatin M (R&D Systems, Minneapolis, MN). Single-cell suspensions were seeded on preplated OP9 stromal cells<sup>15</sup> in the 24-well plate, followed by incubation at 37°C in a 5% CO<sub>2</sub> incubator. Images were visualized with a Nikon Eclipse TE2000-U microscope equipped with 40 $\times$ /0.60 and 10 $\times$ /0.30 NA objective lenses (Nikon, Tokyo, Japan), and were captured with a C5810 camera (Hamamatsu Photonics, Hamamatsu, Japan).

### Plasmid construction

The cDNA of human Runx1 was subcloned into the *EcoRI* restriction site of the retrovirus vector pMYS/internal ribosomal entry site-enhanced green fluorescent protein (IRESEGFP; pMYS/IG).<sup>16</sup> The cDNAs for FLAG-tagged murine SCL and FLAG-tagged murine GATA2 were inserted into the *EcoRI* and *NotI* restriction sites of pMYS/IG. The cDNA for murine *Notch1* intracellular domain (NICD)<sup>3</sup> was subcloned into the *BamHI* restriction site of pMYS/IG. To assess the domain functions of Runx1, we used mutants and wild-type Runx1 constructed in pMY/IG.<sup>14</sup> The pME18S-HA-Runx1 and pME18S-PEBP2 $\beta$  were described previously.<sup>17</sup> The cDNA for FLAG-tagged murine Hes1 was inserted into the *EcoRI* and *NotI* restriction sites of the pME18S-expression vector and in-frame into the *EcoRI* and *XbaI* restriction sites of the p3xFLAG-myc-CMV-25-expression vector (Sigma, St Louis, MO).

### Retroviral transduction

Plat-E packaging cells ( $2 \times 10^6$ )<sup>16</sup> were transiently transfected with 3  $\mu$ g of retrovirus vectors, mixed with 9  $\mu$ L of FuGENE6 (Roche Applied Science, Indianapolis, IN), and incubated at 37°C. Supernatant containing retrovirus was collected 48 hours after transfection and used immediately for infection. Retroviral transduction of the cells derived from *Notch1*-null P-Sp regions was performed as described previously.<sup>14</sup> In brief, the viral supernatant was added to the P-Sp cells seeded on the OP9 stromal-cell layer together with 10  $\mu$ g/mL polybrene (Sigma). After 72 hours of incubation, virus-containing medium was replaced by the original culture medium. The cells were incubated for another 10 days and processed for analysis. To confirm the expression of proteins, NIH3T3 cells were also infected with the same viral supernatants. The efficiency of infection was evaluated by the positivity of GFP. The proteins were detected by Western blot using anti-Runx1 antibody (PC284L; Oncogene, Cambridge, MA), anti-FLAG monoclonal antibody (M2; Sigma), and anti-FLAG polyclonal antibody (F7425; Sigma) to detect Runx1, GATA2, and SCL, respectively. F7425 antibody was used to exclude the overlap of SCL and nonspecific band by M2 antibody.

### CFC assay

The nonadherent or semiadherent cells that emerged from wild-type and *Notch1*-null P-Sp regions were used for colony-forming-cell (CFC) assays. Cells ( $6 \times 10^4$ ) were plated into MethoCult GF M3434 medium (StemCell

Technologies, Vancouver, BC, Canada) and cultured in a 5% CO<sub>2</sub> incubator at 37°C. Colony types were determined at day 7 by morphologic appearance and by Wright-Giemsa staining of each colony. Images were taken with a Nikon Eclipse TE2000-U.

### Flow cytometric analysis

Flow cytometric analysis was performed with a BD LSRII (BD Biosciences, San Jose, CA) after addition of 7-amino-actinomycin D (7-AAD) (Via-Probe; BD Pharmingen, San Diego, CA) to exclude dead cells. For surface staining, cell suspensions collected from the P-Sp cultures were incubated on ice for 30 minutes in the presence of various mixtures of labeled monoclonal antibodies. The following monoclonal antibodies were purchased from BD Pharmingen: phycoerythrin (PE)-conjugated anti-granulocyte 1 (anti-Gr-1), anti-macrophage antigen 1 (anti-Mac-1), anti-stem-cell antigen 1 (anti-Sca-1), anti-Ter-119, allophycocyanin (APC)-conjugated anti-CD45, anti-c-Kit, and biotin-conjugated anti-CD34. Biotinylated antibodies were labeled with PE- or APC-conjugated streptavidin.

### Immunoprecipitation and Western blotting

COS7 cells were transfected with expression plasmids (pME-HA-Runx1 and p3xFLAG-myc-CMV-25-Hes1) using the FuGENE6 according to the manufacturer's instruction. The cells were cultured in Dulbecco modified Eagle medium (DMEM) supplemented with 10% fetal calf serum (FCS) for 48 hours after transfection and were lysed in radioimmunoprecipitation assay (RIPA) buffer.<sup>14</sup> These cell lysates were precleared with protein G-sepharose (Amersham Bioscience, Little Chalfont, United Kingdom) and mixed with anti-FLAG antibody (M2; Sigma) or anti-HA antibody (HA.11; Covance Research Products, Berkeley, CA) for 2 hours. The antibody-associated proteins were then recovered on protein G-sepharose beads. The beads were washed 4 times with the RIPA buffer. Whole-cell lysates containing 100  $\mu$ g of proteins and immunoprecipitates were subjected to 10% sodium dodecyl sulfate-polyacrylamide gel electrophoresis (SDS-PAGE) and transferred to polyvinylidene difluoride membranes (Immobilon; Millipore, Bedford, MA). The membranes were blocked with 5% skim milk treated with either peroxidase-conjugated anti-FLAG monoclonal antibody (M2; Sigma) or peroxidase-conjugated anti-HA monoclonal antibody (12CA5; Roche Applied Science). The blots were visualized using the enhanced chemiluminescence (ECL) system (Amersham Bioscience).

### Transcriptional response assays

Luciferase assays were performed as described previously<sup>18</sup> with minor modifications. Briefly, HeLa cells were transfected with 300 ng of reporter (pM-CSF-R-luc),<sup>19</sup> and expression plasmids (combinations of 200 ng of pME18S-HA-Runx1 and 160 ng of pME18S-PEBP2 $\beta$  and 60, 200, or 600 ng of pME18S-FLAG-Hes1 or control) using FuGENE6 according to the manufacturer's instructions. As a control of transfection efficiency, a plasmid expressing  $\beta$ -galactosidase was cotransfected. The cells were harvested 48 hours after transfection and assayed for luciferase activity. The data were normalized to  $\beta$ -galactosidase activity.

### Quantitative PCR analysis

NIH3T3 cells were infected with NICD or mock retrovirus. The cells were cultured in DMEM medium supplemented with 10% FCS for 48 hours after infection and were selected by the expression of GFP with the FACSAria (BD Biosciences). Total cellular RNA was extracted with RNeasy (QIAGEN, Hilden, Germany) and converted into cDNAs by reverse transcriptase (Superscript III; Invitrogen, Carlsbad, CA). Real-time polymerase chain reaction (PCR) was performed using TaqMan Gene Expression Assays Mm00486762\_m1 (Applied Biosystems, Foster City, CA) with the ABI PRISM 7000 Sequence Detection System (Applied Biosystems) according to the manufacturer's instructions. Amplification of 18S ribosomal RNA cDNA was used as the endogenous normalization standard.

**Results**

**Retroviral expression of Runx1 rescues hematopoietic defects of *Notch1*-null P-Sp regions**

It has been reported that expression of Runx1 or its homolog, *Lozenge*, is up-regulated by positive Notch signaling in zebrafish and *Drosophila* systems, respectively.<sup>10,11</sup> We thus first evaluated whether Notch activation results in up-regulation of Runx1 also in the mammalian system. When NIH3T3 cells were transiently transfected with Notch1 intracellular domain (NICD), which represents the constitutive active form of Notch1, the mRNA level of Runx1 increased (Table 1).

We then examined whether forced expression of Runx1 could rescue the hematopoietic defect of *Notch1*-null mice. Wild-type P-Sp cells gave rise to round-shaped nonadherent cells when overlaid on the OP9 stromal cells. Flow cytometric analysis of these cells revealed that they were viable (7-AAD negative) CD45-positive cells (top panels in Figure 1A), representing hematopoietic cells. No such cells were generated from *Notch1*-null P-Sp cells and only background OP9 cells were observed (bottom panels in Figure 1A).<sup>3</sup> We retrovirally infected *Notch1*-null P-Sp cells that were seeded on the OP9 layer with Runx1, SCL, or GATA2, and assessed whether *Notch1*-null P-Sp cells could generate hematopoietic cells. Titers of the retroviruses containing Runx1, SCL, and GATA2 were similar to each other as evaluated by infecting NIH3T3 cells with these viruses (Figure 2A). Expression of individual proteins was confirmed by a Western blot analysis (Figure 2B). Mock, SCL, and GATA2 transduction did not generate round-shaped nonadherent cells morphologically or viable CD45-positive cells detectable by flow cytometric analysis. In contrast, Runx1-transduced P-Sp cells gave rise to round-shaped nonadherent cells. These cells were shown to be viable CD45-positive cells by flow cytometric analysis (Figure 1B). This pattern was identical to the positive control (*Notch1*<sup>+/+</sup> P-Sp cells; top panels in Figure 1A).

To confirm that the cells developed from Runx1-infected *Notch1*-null P-Sp cells (hereafter referred to as Runx1-rescued cells) retain the features of hematopoietic cells, we evaluated these cells for surface markers and CFC activities. The flow cytometric analysis of the Runx1-rescued cells at day 12 revealed that they express hematopoietic cell-surface markers such as a panleukocyte marker (CD45), stem-cell markers (c-Kit, CD34, and Sca1), myeloid-cell markers (Gr-1 or Mac-1), and an erythroid-cell marker (Ter-119) (Figure 3A). Their expression profiles were reminiscent of those of hematopoietic cells generated from the wild-type P-Sp cells (Figure 3B). The P-Sp culture system faithfully reproduced the generation of hematopoietic cells, and there were no consistent differences between Runx1-rescued and wild-

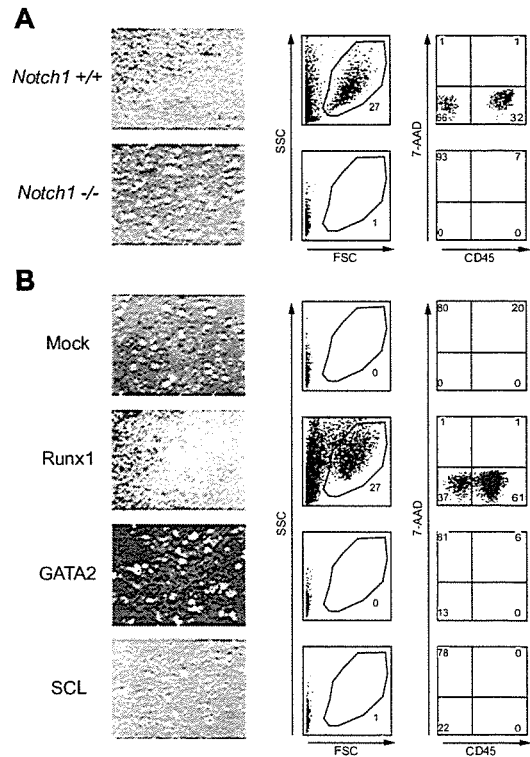


**Figure 1. Retroviral expression of Runx1 rescues hematopoietic defect of *Notch1*-null P-Sp region.** (A) P-Sp cells from wild-type (*Notch1*<sup>+/+</sup>) and *Notch1*-null (*Notch1*<sup>-/-</sup>) embryos at E9.5 were cultured for 5 days on OP9 cells. (B) P-Sp cells from *Notch1*-null embryos at E9.5 were infected with mock retrovirus or retrovirus containing Runx1, SCL, or GATA2, and cultured for 12 days on OP9 cells. Microscopic representation (left column; original magnification, × 100). Only cocultured OP9 cells are shown if hematopoietic cells are not produced. Flow cytometric analyses (center and right columns) of cells generated in the culture. Percentages of cells gated (center columns) and cells in each quadrant (right columns) are indicated.

type P-Sp-derived cells in the surface-marker expression levels, although we observed variable minor differences in individual experiments partly because of the variation in the time required for hematopoietic development (Figure 3A-B).

When the Runx1-rescued cells were seeded into semisolid medium at day 12 and cultured for an additional 7 days, they generated mixed, granulocyte/macrophage, and erythroid colonies containing enucleated erythrocytes (Figure 4A) at a frequency comparable to that of wild-type P-Sp-derived cells (Figure 4B-C). There were no statistical differences in the numbers of total ( $P = .11$ ) and individual (erythroid,  $P = .20$ ; granulocyte/macrophage,  $P = .11$ ; mixed,  $P = .07$ ) colonies generated from *Notch1*<sup>+/+</sup>

**Table 1. Notch activation up-regulates the expression of Runx1**

	RAU	Mean	Notch-mock
<b>Experiment 1</b>			2.78*
NIH3T3-Mock	0.112634; 0.077514; 0.093663	0.094604	
NIH3T3-Notch	0.263982; 0.241864; 0.282636	0.262827	
<b>Experiment 2</b>			4.12*
NIH3T3-Mock	0.038500; 0.045755; 0.044123	0.042792	
NIH3T3-Notch	0.186016; 0.148638; 0.194443	0.176366	

Data are from 2 independent experiments in triplicate. RAU, relative arbitrary units; Notch-mock, the ratio of RAU by constitutive active Notch 1 infection and RAU by mock infection.

\* $P < .01$  (2-tailed, unequal variance *t* test).

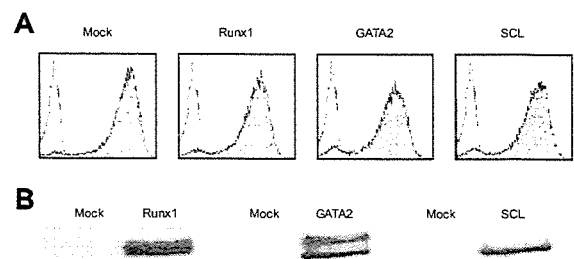


**Figure 2. Retroviruses properly create Runx1, GATA2, and SCL proteins.** (A) The efficiency of retrovirus-mediated gene transfer of Runx1, GATA2, or SCL was estimated by infecting NIH3T3 cells. Retrovirus-infected cells were evaluated by the expression of GFP (shaded histograms). Uninfected NIH3T3 cells are also shown as a control (open histograms). (B) Expression of individual proteins was confirmed by a Western blot analysis.

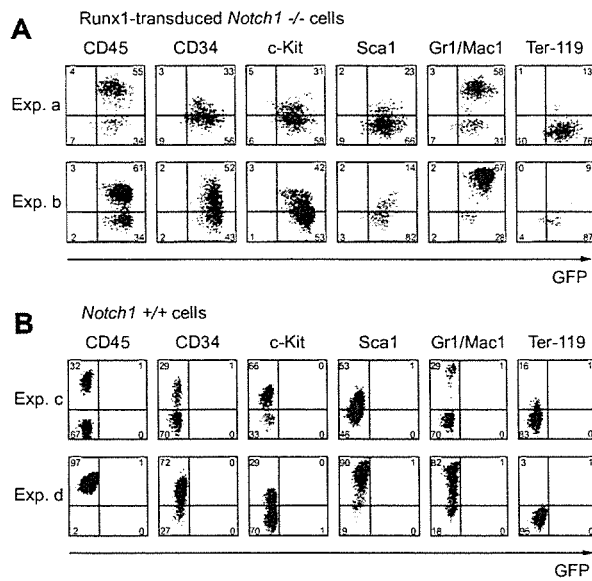


**Figure 3. Runx1-rescued cells express hematopoietic surface markers.** Expression of hematopoietic surface markers of cultured cells at day 12 from Runx1-transduced *Notch1*<sup>-/-</sup> embryos (A) or wild-type (*Notch1*<sup>+/+</sup>) embryos (B) was evaluated by flow cytometric analyses. GFP intensity (marking retrovirus-transduced cells) is plotted on the x-axis and intensity of counterstaining of hematopoietic surface markers is plotted on the y-axis. The results show representative results of independent replicates from 5 experiments. Percentages of cells in each quadrant are indicated.

and Runx1-transduced *Notch1*<sup>-/-</sup> P-Sp-derived cells. These observations indicate that the hematopoietic characteristics of Runx1-rescued cells were similar to those of wild-type P-Sp-derived cells.

#### Functional implication of Runx1 at the downstream of Notch-RBP-J $\kappa$ pathway

Runx1 has several distinct domains with defined biochemical functions. The Runt domain mediates both binding to DNA and dimerization with a partner protein, CBF $\beta$ /PEBP2 $\beta$ , whereas the transactivation domain interacts with transcriptional coactivators. Inhibitory domain counteracts the effect of the transactivation domain. The VWRPY motif located near the C-terminus mediates the interaction with a corepressor, TLE. A domain that interacts with mSin3A corepressor is also identified.<sup>9</sup> To assess whether Runx1 functions as an activator or a repressor<sup>20</sup> to restore the hematopoietic defect of *Notch1*-null embryo, we examined a series of Runx1 mutants (Figure 5)<sup>14</sup> for hematopoietic rescue.

Infection of retroviruses containing wild-type and several mutants,  $\Delta$ 444,  $\Delta$ 397, and  $\Delta$ 205-332 of Runx1 (Figure 5) resulted in the rescue of the *Notch1*-null phenotype, giving the same pattern with the culture of wild-type P-Sp cells (Figure 1A, top panels). In contrast, other mutants,  $\Delta$ 335,  $\Delta$ 288, AML1a,  $\Delta$ RD,  $\Delta$ 205-332, and R139G (Figure 5) could not rescue the *Notch1*-null phenotype, giving the same pattern with the negative control (Figure 1A, bottom panels). Therefore, wild-type of Runx1 and the mutants that lack the VWRPY domain ( $\Delta$ 444,  $\Delta$ 397) or the mSin3A-binding region ( $\Delta$ 181-210) could restore the production of hematopoietic cells in the *Notch1*-null P-Sp culture, whereas those mutants that lack transactivation domain ( $\Delta$ 335,  $\Delta$ 288, AML1a, and  $\Delta$ 205-332) or Runt domain ( $\Delta$ RD) could not rescue hematopoiesis from the *Notch1*-null P-Sp cells. Since changes in the tertiary structure of the protein could influence the function independent of the role of each domain, we also examined R139G, a mutant isolated from a

patient with myelodysplastic syndrome (MDS) that harbors a point mutation causing substitution of Arg139 in the Runt domain with Gly. The DNA-binding ability is severely impaired in R139G, although the ability to heterodimerize with CBF $\beta$ /PEBP2 $\beta$  is spared.<sup>21</sup> This mutant could not restore hematopoiesis. These results suggest that, in the presence of an intact Runt domain, the transcriptional activating function is necessary and sufficient for Runx1 to rescue the hematopoietic defect of *Notch1*-null mice in the P-Sp culture system, while the transcriptional repressing function is dispensable.

#### Notch signaling also regulates transactivating function of Runx1

*Hes1* is known to be a canonical Notch-RBP-J $\kappa$  target gene in mammals. It is also evident, however, by a number of studies that *Hes1* mediates a part of, but not the whole, Notch-RBP-J $\kappa$  signaling.<sup>22</sup> In adult hematopoiesis, *Hes1* maintains HSCs in vitro and expands them in vivo when retrovirally introduced to a highly HSC-enriched population.<sup>23</sup> Because *Hes1* is expressed in the hematopoietic clusters budding from the dorsal aorta,<sup>8</sup> this transcription factor is a candidate as a physiologic target of the Notch-RBP-J $\kappa$  pathway in the embryonic hematopoietic development. *Hes1* has also been known to mediate cross-talk between Notch and

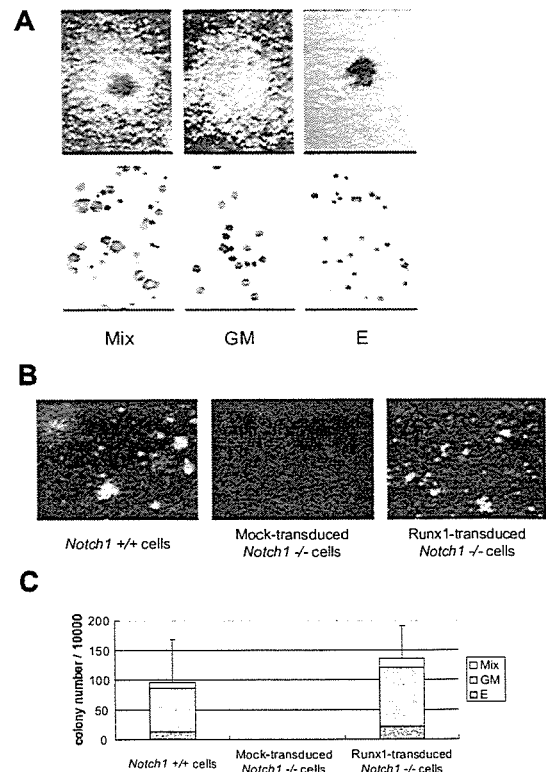


**Figure 4. Runx1-rescued cells generate hematopoietic colonies.** Colony formation of the Runx1-rescued cells from *Notch1*-null embryos. The rescued cells were harvested at day 12 and plated into MethoCult GF M3434 medium. (A) Representative hematopoietic colonies at day 7 are shown. Mix indicates mixed colony; GM, granulocyte/macrophage colony; and E, erythroid colony. Morphology of the colonies (top panels); original magnification,  $\times$  100. Wright-Giemsa-stained cytospin preparation of corresponding cell populations (bottom panels); original magnification,  $\times$  600. (B) Photographs of representative colonies. Original magnification,  $\times$  3. (C) The total number of colonies and the frequencies of different kinds of colonies. The results show the mean values of 5 independent experiments, each in duplicate, with standard deviations for the total colony numbers. Data were statistically analyzed by 2-tailed, unequal-variance *t* test.

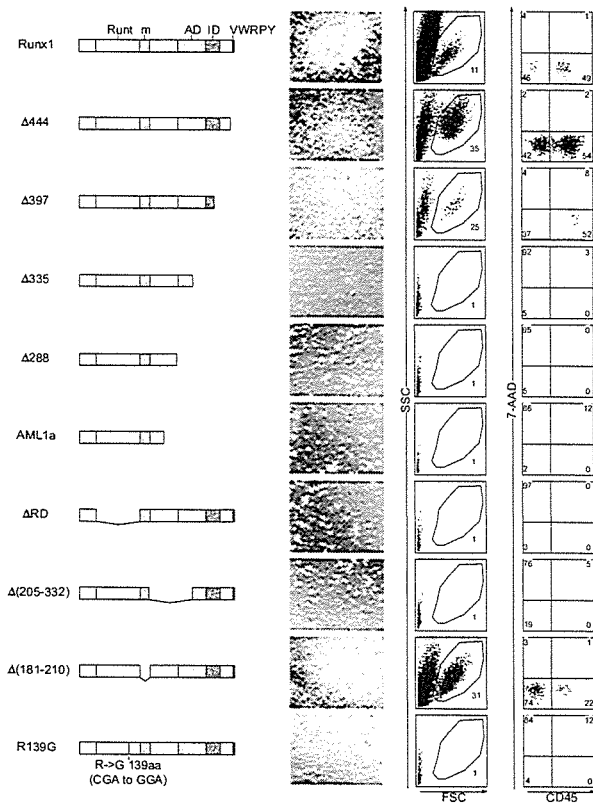


**Figure 5. The transcriptionally active form of Runx1 is required for hematopoietic rescue.** P-Sp cells from *Notch1*-null embryos at E 9.5 were infected with retroviruses containing *Runx1* mutants and cultured on OP9 cells for 12 days. Structures of *Runx1* mutants are depicted (left column). Runt indicates the Runt domain; m, a binding region for mSin3A; AD, transactivation domain; ID, inhibitory domain; and VWRPY, VWRPY motif. Microscopic representations (center column; original magnification,  $\times 100$ ) and flow cytometric analyses (right 2 columns) of cells produced in the culture. Percentages of cells gated (center columns) and cells in each quadrant (right columns) are indicated.

other signaling pathways such as Janus-activating kinase/signal transducer and activator of transcription (JAK/STAT), Wnt, and Ras/mitogen-activated protein kinase (MAPK) pathways.<sup>24-26</sup> Furthermore, the transactivating function of Runx2, another Runx family member, is modified by Hes proteins and their relatives Hey proteins. When overexpressed, Hes1 potentiates Runx2-mediated transactivation in the transfected cells,<sup>27</sup> while Hey represses Runx2-mediated transactivation.<sup>28,29</sup>

Based on these pieces of information, we assessed whether Hes1 also modulates Runx1-mediated transactivation. Consistent with a previous report in which Hes1 was shown to bind to Runx1 in glutathione S-transferase (GST) pull-down assays,<sup>27</sup> we detected HA-tagged Runx1 protein in the anti-FLAG immunoprecipitant, and reversely, FLAG-tagged Hes1 protein in the anti-HA immunoprecipitant, indicating physical interaction of Hes1 with Runx1 (Figure 6A). Moreover, Hes1 potentiated Runx1-mediated transactivation when expressed in HeLa cells, depending on the expression levels of Hes1 (Figure 6B).

## Discussion

In this study, we showed that Runx1 rescues the defective hematopoiesis of *Notch1*-null mice in the OP9 culture system. The functional relationship between Notch and Runx families during

hematopoietic development was first indicated in *Drosophila*, in which Notch up-regulates the expression of a *Runx* family gene, *Lozenge*.<sup>10</sup> More recently, it was shown that a zebrafish Notch-signaling mutant *mind bomb* fails in the specification of definitive HSCs during embryogenesis, and that Runx1 is required for expansion of HSCs in the zebrafish AGM region sufficient to restore the HSC specification in the *mind bomb* mutant.<sup>11</sup> The data shown in the present study strongly indicate that the Notch-Runx pathway is conserved from invertebrates to mammals and that Runx1 locates at a very proximal position in the Notch1 signaling pathway during establishment of definitive hematopoiesis.

GATA2 is also reported to have an important role downstream of Notch signaling in the establishment of definitive hematopoiesis. It was reported that NICD directly binds to the *Gata2* promoter and increases its expression level in mouse AGM cells.<sup>8</sup> Similarly in *Drosophila*, Notch up-regulates *Serpent* and induces emergence of hemocyte progenitors in lymph glands.<sup>12</sup> In our retroviral expression system, however, GATA2 could not rescue the hematopoietic defect of *Notch1*-null P-Sp cells (Figure 1B). It remains unknown whether GATA2 expression in more regulated levels and/or timings could rescue the hematopoietic deficient phenotype of *Notch1*-knockout P-Sp cells.

We clearly demonstrated that definitive hematopoiesis is rescued by forced expression of Runx1 in the *Notch1*-null P-Sp cells, but it should be directly shown whether transplantable HSCs are generated from the *Notch1*-null Runx1-introduced P-Sp cells. Fresh P-Sp cells obtained from wild-type embryos can be engrafted

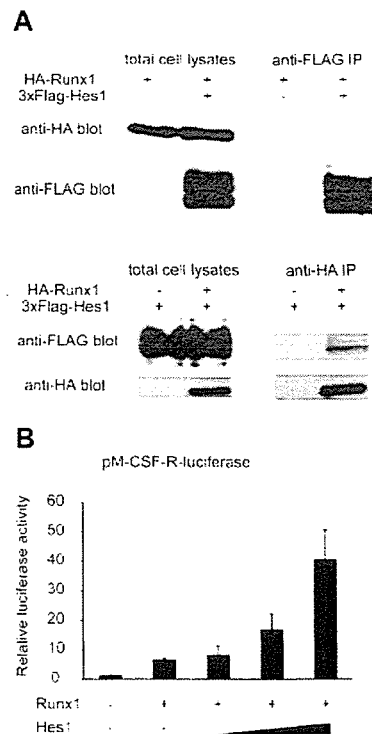


**Figure 6. Notch signaling regulates transcriptional level of Runx1 and modulates the function of Runx1 protein through the effector protein, Hes1.** (A) COS7 cells were transfected with HA-tagged Runx1 and 3xFLAG-tagged Hes1. Whole-cell extracts were immunoprecipitated (IP) with anti-FLAG antibody or anti-HA antibody followed by immunoblotting (blot) using anti-HA antibody or anti-FLAG antibody. (B) Relative luciferase activity in HeLa cells transfected with Runx1 (200 ng) and Runx1-dependent macrophage colony-stimulating factor receptor (pM-CSF-R) luciferase reporter (300 ng) with or without cotransfection of Hes1 (60, 200, or 600 ng). Data are means  $\pm$  standard errors of duplicate wells in a representative experiment. Reproducible results were obtained in 3 independent experiments.

to mouse bone marrow if injected in the preconditioned newborn mice, as described.<sup>3,30</sup> It is unknown, however, whether the cultured P-Sp cells are also engraftable with the same method. We were unable to observe engraftment of the cultured P-Sp cells unlike fresh P-Sp cells, when injected to busulfan-pretreated newborn mice (data not shown). Culturing the cells, even for just a short time, is prerequisite for the retroviral gene transfer, which stands as a major technical obstacle to assess the engraftability of the *Notch1*-null Runx1-introduced P-Sp cells. Transgenic expression of Runx1, under an appropriate promoter, in the *Notch1*-null background may reveal further that the *Notch1*-Runx1 pathway represents an essential physiologic channel for the mammalian HSC generation from the P-Sp cells.

We also showed that *Hes1*, a known mediator of Notch signaling, cooperatively activates the Runx1-responsive pM-CSF-R luciferase reporter. This observation suggests that the *Notch1* pathway modulates expression of Runx1 target genes through multiple mechanisms. There is a possibility that *Notch1*

directly augments the expression of Runx1 target genes. Although overexpression of Runx1 is sufficient to restore hematopoietic potential in *Notch1*-null P-Sp cells, both of these mechanisms might cooperatively contribute to HSC generation during normal development.

## Acknowledgments

We thank M. Ohki for the gift of the human Runx1 cDNA, Y. Ito for the PEBP2 $\beta$  cDNA, D.-E. Zhang for the pM-CSF-R-luc vector, T. Kitamura for the Plat-E packaging cells and the pMYs/IRES-EGFP retrovirus vector, T. Nakano for the OP9 stromal cells, R. Kageyama for the *Hes1* cDNA, and Kirin Brewery Pharmaceutical Research Laboratory for the cytokines. We dedicate this paper for the late Prof Hisamaru Hirai, who passed away during the progress of this study.

## References

- Cumano A, Dieterlen-Lievre F, Godin I. Lymphoid potential, probed before circulation in mouse, is restricted to caudal intraembryonic splanchnopleura. *Cell*. 1996;86:907-916.
- Godin IE, Garcia-Porrero JA, Coutinho A, Dieterlen-Lievre F, Marcos MA. Para-aortic splanchnopleura from early mouse embryos contains B1a cell progenitors. *Nature*. 1993;364:67-70.
- Kumano K, Chiba S, Kunisato A, et al. *Notch1* but not *Notch2* is essential for generating hematopoietic stem cells from endothelial cells. *Immunity*. 2003;18:699-711.
- Artavanis-Tsakonas S, Rand MD, Lake RJ. Notch signaling: cell fate control and signal integration in development. *Science*. 1999;284:770-776.
- Okuda T, van Deursen J, Hiebert SW, Grossfeld G, Downing JR. AML1, the target of multiple chromosomal translocations in human leukemia, is essential for normal fetal liver hematopoiesis. *Cell*. 1996;84:321-330.
- Porcher C, Swat W, Rockwell K, Fujiwara Y, Alt FW, Orkin SH. The T cell leukemia oncoprotein SCL/tal-1 is essential for development of all hematopoietic lineages. *Cell*. 1996;86:47-57.
- Tsai FY, Keller G, Kuo FC, et al. An early hematopoietic defect in mice lacking the transcription factor GATA-2. *Nature*. 1994;371:221-226.
- Robert-Moreno A, Espinosa L, de la Pompa JL, Bigas A. RBPjkappa-dependent Notch function regulates Gata2 and is essential for the formation of intra-embryonic hematopoietic cells. *Development*. 2005;132:1117-1126.
- Kurokawa M, Hirai H. Role of AML1/Runx1 in the pathogenesis of hematological malignancies. *Cancer Sci*. 2003;94:841-846.
- Lebestky T, Jung SH, Banerjee U. A Serrate-expressing signaling center controls *Drosophila* hematopoiesis. *Genes Dev*. 2003;17:348-353.
- Burns CE, Traver D, Mayhall E, Shepard JL, Zon LI. Hematopoietic stem cell fate is established by the *Notch*-*Runx* pathway. *Genes Dev*. 2005;19:2331-2342.
- Mandal L, Banerjee U, Hartenstein V. Evidence for a fruit fly hemangioblast and similarities between lymph-gland hematopoiesis in fruit fly and mammal aorta-gonadal-mesonephros mesoderm. *Nat Genet*. 2004;36:1019-1023.
- Conlon RA, Reaume AG, Rossant J. *Notch1* is required for the coordinate segmentation of somites. *Development*. 1995;121:1533-1545.
- Goyama S, Yamaguchi Y, Imai Y, et al. The transcriptionally active form of AML1 is required for hematopoietic rescue of the AML1-deficient embryonic para-aortic splanchnopleural (P-Sp) region. *Blood*. 2004;104:3558-3564.
- Nakano T, Kodama H, Honjo T. Generation of lymphohematopoietic cells from embryonic stem cells in culture. *Science*. 1994;265:1098-1101.
- Kitamura T, Koshino Y, Shibata F, et al. Retrovirus-mediated gene transfer and expression cloning: powerful tools in functional genomics. *Exp Hematol*. 2003;31:1007-1014.
- Tanaka K, Tanaka T, Kurokawa M, et al. The AML1/ETO(MTG8) and AML1/Evi-1 leukemia-associated chimeric oncoproteins accumulate PEBP2beta(CBFbeta) in the nucleus more efficiently than wild-type AML1. *Blood*. 1998;91:1688-1699.
- Imai Y, Kurokawa M, Yamaguchi Y, et al. The corepressor mSin3A regulates phosphorylation-induced activation, intranuclear location, and stability of AML1. *Mol Cell Biol*. 2004;24:1033-1043.
- Zhang DE, Hetherington CJ, Meyers S, et al. CCAAT enhancer-binding protein (C/EBP) and AML1 (CBF alpha2) synergistically activate the macrophage colony-stimulating factor receptor promoter. *Mol Cell Biol*. 1996;16:1231-1240.
- Durst KL, Hiebert SW. Role of RUNX family members in transcriptional repression and gene silencing. *Oncogene*. 2004;23:4220-4224.
- Imai Y, Kurokawa M, Izutsu K, et al. Mutations of the AML1 gene in myelodysplastic syndrome and their functional implications in leukemogenesis. *Blood*. 2000;96:3154-3160.
- Kageyama R, Ohtsuka T, Hatakeyama J, Ohsawa R. Roles of bHLH genes in neural stem cell differentiation. *Exp Cell Res*. 2005;306:343-348.
- Kunisato A, Chiba S, Nakagami-Yamaguchi E, et al. HES-1 preserves purified hematopoietic stem cells ex vivo and accumulates side population cells in vivo. *Blood*. 2003;101:1777-1783.
- Devgan V, Mammucari C, Millar SE, Briskin C, Dotto GP. p21WAF1/Cip1 is a negative transcriptional regulator of Wnt4 expression downstream of *Notch1* activation. *Genes Dev*. 2005;19:1485-1495.
- Kamakura S, Oishi K, Yoshimatsu T, Nakafuku M, Masuyama N, Gotoh Y. *Hes* binding to STAT3 mediates crosstalk between Notch and JAK-STAT signalling. *Nat Cell Biol*. 2004;6:547-554.
- Stockhausen MT, Sjolund J, Axelson H. Regulation of the Notch target gene *Hes-1* by TGFalpha induced Ras/MAPK signaling in human neuroblastoma cells. *Exp Cell Res*. 2005;310:218-228.
- McLarren KW, Lo R, Grbavec D, Thirunavukkarasu K, Karsenty G, Stifani S. The mammalian basic helix loop helix protein HES-1 binds to and modulates the transactivating function of the runt-related factor Cbfa1. *J Biol Chem*. 2000;275:530-538.
- Zamurovic N, Cappellen D, Rohner D, Susa M. Coordinated activation of notch, Wnt, and transforming growth factor-beta signaling pathways in bone morphogenic protein 2-induced osteogenesis. Notch target gene *Hey1* inhibits mineralization and Runx2 transcriptional activity. *J Biol Chem*. 2004;279:37704-37715.
- Garg V, Muth AN, Ransom JF, et al. Mutations in NOTCH1 cause aortic valve disease. *Nature*. 2005;437:270-274.
- Yoder MC, Hiatt K, Dutt P, Mukherjee P, Bodine DM, Orlic D. Characterization of definitive lymphohematopoietic stem cells in the day 9 murine yolk sac. *Immunity*. 1997;7:335-344.

# Genomewide Screening of DNA Copy Number Changes in Chronic Myelogenous Leukemia with the Use of High-Resolution Array-Based Comparative Genomic Hybridization

Noriko Hosoya,<sup>1,2</sup> Masashi Sanada,<sup>1</sup> Yasuhito Nannya,<sup>1</sup> Kumi Nakazaki,<sup>1</sup> Lili Wang,<sup>1</sup> Akira Hangaishi,<sup>1</sup> Mineo Kurokawa,<sup>1</sup> Shigeru Chiba,<sup>1,2</sup> and Seishi Ogawa<sup>1,3,4\*</sup>

<sup>1</sup>Department of Hematology and Oncology, Graduate School of Medicine, University of Tokyo, Tokyo, Japan

<sup>2</sup>Department of Cell Therapy and Transplantation Medicine, University of Tokyo Hospital, University of Tokyo, Tokyo, Japan

<sup>3</sup>Department of Regeneration Medicine for Hematopoiesis, Graduate School of Medicine, University of Tokyo, Tokyo, Japan

<sup>4</sup>Core Research for Evolutional Science and Technology, Japan Science and Technology Corporation, Saitama, Japan

Chronic myelogenous leukemia (CML) evolves from an indolent chronic phase (CP) characterized by the Philadelphia chromosome. Without effective therapy, it progresses to an accelerated phase (AP) and eventually to a fatal blast crisis (BC). To identify the genes involved in stage progression in CML, we performed a genomewide screening of DNA copy number changes in a total of 55 CML patients in different stages with the use of the high-resolution array-based comparative genomic hybridization (array CGH) technique. We constructed Human IM arrays that contained 3,151 bacterial artificial chromosome (BAC) DNAs, allowing for an average resolution of 1.0 Mb across the entire genome. In addition to common chromosomal abnormalities, array CGH analysis unveiled a number of novel copy number changes. These alterations included losses in 2q26.2–q37.3, 5q23.1–q23.3, 5q31.2–q32, 7p21.3–p11.2, 7q31.1–q31.33, 8pter–p12(p11.2), 9p, and 22q13.1–q13.31 and gains in 3q26.2–q29, 6p22.3, 7p15.2–p14.3, 8p12, 8p21.3, 8p23.2, 8q24.13–q24.21, 9q, 19p13.2–p12, and 22q13.1–q13.32 and occurred at a higher frequency in AP and BC. Minimal copy number changes affecting even a single BAC locus were also identified. Our data suggests that at least a proportion of CML patients carry still-unknown cryptic genomic alterations that could affect a gene or genes of importance in the disease progression of CML. This article contains Supplementary Material available at <http://www.interscience.wiley.com/jpages/1045-2257/suppmat>. © 2006 Wiley-Liss, Inc.

## INTRODUCTION

Chronic myelogenous leukemia (CML) is a clonal disorder originating from pluripotent hematopoietic stem cells that is characterized by the Philadelphia (Ph) chromosome generated by the  $t(9;22)(q34;q11)$  (Rowley, 1973; Melo et al., 2003). CML typically shows 3 clinical stages: the initial indolent chronic phase (CP), followed by the intermediate accelerated phase (AP), and then the terminal fatal stage, blast crisis (BC). The prognosis of patients in BC is still very poor, with a median survival of only a few months (Calabretta and Perrotti, 2004). At present, no promising curative therapeutic options are available for patients in BC. The recent development of imatinib mesylate, which selectively inhibits enhanced tyrosine kinase activity of the chimeric BCR–ABL oncoprotein generated by the Ph chromosome, produced impressive therapeutic effects on patients in CP. However, the benefits from this drug seem short-lived once patients progressed to BC (Calabretta and Perrotti, 2004). Thus, to develop new ther-

apeutic approaches for patients in BC, it is essential to identify molecular targets of blastic transformation.

The BC stage of CML is commonly associated with nonrandom secondary chromosomal changes that, in addition to the  $t(9;22)$ , include +Ph, +8,  $i(17q)$ , +19,  $t(3;21)(q26;q22)$ , and  $t(7;11)(p15;p15)$  (Prigogina et al., 1978; Alimena et al., 1987; Blick et al., 1987; Melo et al., 2003), or with mutations in

Supported by: Grant-in-Aid for Scientific Research on Priority Areas, Ministry of Education, Culture, Sports, Science and Technology (MEXT); Grant number: KAKENHI 17013022, Grant-in-Aid for Scientific Research, Japan Society for the Promotion of Science (JSPS); Grant number: KAKENHI 16390272, Research on Human Genome, Tissue Engineering, Health and Labour Sciences Research Grants, Ministry of Health, Labour and Welfare; Japan Health Sciences Foundation.

\*Correspondence to: Seishi Ogawa, Department of Hematology and Oncology, Department of Regeneration Medicine for Hematopoiesis, Graduate School of Medicine, University of Tokyo, 7-3-1, Hongo, Bunkyo-ku, Tokyo 113-8655, Japan.  
E-mail: [sogawa-ty@umin.ac.jp](mailto:sogawa-ty@umin.ac.jp)

Received 19 October 2005; Accepted 22 November 2005

DOI 10.1002/gcc.20303

Published online 19 January 2006 in Wiley InterScience (www.interscience.wiley.com).

the *TP53*, *CDKN2A*, *RBI*, or *RAS* genes (Ahuja et al., 1989; Kelman et al., 1989; LeMaistre et al., 1989; Feinstein et al., 1991; Nakai et al., 1992, 1994; Mitani et al., 1994; Nakai and Misawa, 1995; Sill et al., 1995; Nakamura et al., 1996; Fioretos et al., 1999; Beck et al., 2000). However, the molecular mechanisms responsible for disease progression in CML have not been fully understood. Array-based comparative genomic hybridization (array CGH) is a robust technology in which a large number of genomic clones are spotted on a glass slide and comparatively hybridized to differentially labeled tumor and reference DNA to enable high-resolution analysis of copy number changes in cancer genomes (Pinkel et al., 1998). Although the array CGH technique has been drawing increasing attention as a tool for studying alterations of genomes in various tumors (Albertson and Pinkel, 2003), it had not been applied to the analysis of patients with CML.

In the present study, to identify genes underlying stage progression in CML, we manufactured Human 1M arrays containing 3,151 bacterial artificial chromosome (BAC) DNAs and performed CGH analysis in 55 primary CML samples in different stages using these arrays. A number of previously unrecognized small cryptic genomic regions were identified.

## MATERIALS AND METHODS

### PATIENTS AND SAMPLES

After obtaining informed consent, bone marrow or peripheral-blood samples were obtained from 55 Japanese patients diagnosed with CML. Twenty-five of the patients were in the CP stage, 4 were in the AP stage, and 26 were in the BC stage. Clinical details are summarized in Table 1. After approval by the ethical committee at the University of Tokyo, all the samples were subjected to extraction of genomic DNA and anonymized to be used for further analysis according to the regulation of the Japanese government.

### Array Fabrication

We constructed Human 1M arrays containing a subset of the FISH (fluorescence in situ hybridization) Mapped Clones V1.3 collection, which were obtained from BACPAC Resources Center (Children's Hospital Oakland Research Institute, Oakland, CA). After excluding clones missing mapping information, a total of 3,151 clones were finally selected for fabrication of Human 1M arrays (Supple-

mentary Table 1; Supplementary material for this article can be found at <http://www.interscience.wiley.com/jpages/1045-2257/suppmat>), which could be used for genomewide copy number detection at an average resolution of approximately 1.0 Mb. Each BAC DNA was amplified with degenerated oligonucleotide-primed PCR (DOP-PCR) according to the protocol published by Fiegler et al. (2003), with the minor modification of an equimolar combination of DOP 1, 2, and 3 primers being used in the first PCR cycles. Amplified DNA was spotted in duplicate onto GAPS<sup>TM</sup> II coated slides (Corning, International K.K., Tokyo, Japan), using an Affymetrix 419 Arrayer (Affymetrix, Santa Clara, CA). Before hybridization, array slides were briefly rehydrated over steam and immediately dried on a 75°C heat block. After being baked in a drying oven at 65°C for 3 h and UV-crosslinked at 60 mJ, the slides were rinsed with 0.2× standard saline citrate (SSC) and then with distilled water. The reactive moieties of amino-silane remaining on the glass surface were inactivated for 20 min by gently shaking arrays in a blocking solution, which was freshly prepared by dissolving 4.15 g of succinic anhydride in 245 ml of 1-methyl-2-pyrrolidone and then adding 22.5 ml of sodium borate (1M, pH 8.0). The slides were briefly rinsed with distilled water and preserved in a desiccator at room temperature, and immediately before hybridization, they were treated in boiling water for 2 min, placed in 100% cold ethanol, and then dried by centrifugation.

### DNA Labeling and Hybridization to BAC Arrays

Genomic DNA was extracted from mononuclear cells of the bone marrow or peripheral blood of normal individuals using a PUREGENE<sup>TM</sup> DNA Isolation Kit (Gentra Systems, Minneapolis, MN). One microgram each of normal reference genomic (male or female) and test DNA were labeled with Cy3-dUTP and Cy5-dUTP, respectively, using a BioPrime<sup>®</sup> Array CGH Genomic Labeling System (Invitrogen, Carlsbad, CA). After overnight incubation at 37°C, unincorporated nucleotides were removed by use of a BioPrime<sup>TM</sup> Array CGH Purification Module (Invitrogen, Carlsbad, CA). The labeled test and reference DNA were ethanol-precipitated together with 80 µg of human Cot-1 DNA (Invitrogen, Carlsbad, CA) and 100 µg of yeast tRNA (Roche, Basel, Switzerland), redissolved in a hybridization mix [50% formamide, 5% dextran sulfate, 2× SSC, 5% Tris (pH 7.4), 0.1% Tween 20], and denatured at 75°C for 15 min. After incubation at 37°C for 30 min, the mixture was

TABLE 1. Patient Characteristics, Cytogenetic Description of Their Karyotypes, and Presence of BCR/ABL Confirmed by FISH or RT-PCR

Case No.	Sex	Age	Stage	Phenotype	Blast(%)	Karyotype	Methods of BCR/ABL detection
AP1	M	51	CML AP		6	46,XY,t(9;22)(q34;q11)(20/20)	NS
AP2	F	56	CML AP		2	50,XX,t(9;22)(q34;q11)+13,+19,+21,+22(8/15) 51,XX,t(9;22)(q34;q11),+t(9;22),+13,+19,+21,+22(4/15) 52,XX,+8,t(9;22)(q34;q11),+t(9;22),+13,+19,+21,+22(2/15) 47,XX,t(9;22)(q34;q11),+19,-20,-21,+der(22)t(9;22),+mar(1/15)	FISH and RT-PCR
AP3	M	37	CML AP		3.3	46,XY,t(9;22)(q34;q11)(18/20) 47,XY,+8,t(9;22)(q34;q11)(2/20)	RT-PCR
AP4	M	74	CML AP		9	46,XY,t(9;22)(q34;q11)(14/20) 45,XY,-21,t(9;22)(q34;q11)(5/20) 45,XY,-17,t(9;22)(q34;q11)(1/20)	RT-PCR
BC1	M	78	CML BC	ND	30	46,XY,t(9;22)(q34;q11)	NS
BC2	M		CML BC	ND	72	46,XY,t(9;22)(q34;q12)	NS
BC3	M	65	CML BC	lymphoid	90	46,XY,t(9;22)(q34;q11)	NS
BC4	M	33	CML BC	lymphoid	70	NA	NS
BC5	M		CML BC	lymphoid	65	NA	NS
BC6	F	48	CML BC	lymphoid	56	46,XX,t(9;22)(q34;q11)	NS
BC7	F	42	CML BC	lymphoid	60	46,XX,t(9;22)(q34;q11)	NS
BC8	F	42	CML BC	lymphoid	70	46,XX,t(9;22)(q34;q11)	NS
BC9	F	60	CML BC	myeloid	98	46,XX,t(9;22)(q34;q11)	NS
BC10	M	62	CML BC	myeloid	90	46,XY,t(9;22)(q34;q11)	NS
BC11	F		CML BC	myeloid	60	NA	NS
BC12	F	53	CML BC	myeloid	20	NA	NS
BC13	F		CML BC	myeloid	88	NA	NS
BC14	M		CML BC	myeloid	75	NA	NS
BC15	M	46	CML BC	myeloid	70	46,XY,t(9;22)(q34;q11)	NS
BC16	M	67	CML BC	myeloid	73	48,XY,t(3;21;18)(q21;q22;p11),+8,t(9;22)(q34;q11),+12(20/20)	FISH and RT-PCR
BC17	F	57	CML BC	myeloid	39	46,XY,t(9;22)(q34;q11)(10/10)	NS
BC18	M	51	CML BC	myeloid	86	46,XY,t(9;22)(q34;q11)(20/20)	FISH and RT-PCR

(Continued)



TABLE 1. Patient Characteristics, Cytogenetic Description of Their Karyotypes, and Presence of BCR/ABL Confirmed by FISH or RT-PCR (Continued)

Case No.	Sex	Age	Stage	Phenotype	Blast(%)	Karyotype	Methods of BCR/ABL detection
BC19	M	54	CML BC	myeloid	13	NA	FISH and RT-PCR
BC20	M	69	CML BC	myeloid	35	46,XY,t(9;22)(q34;q11)(13/20) 46,XY,t(9;22)(q34;q11),der(12)t(1;12)(q12;q24)(3/20) 46,XY,t(9;22)(q34;q11),der(19)t(1;19)(q12;p13)(4/20)	FISH and RT-PCR
BC21	M	71	CML BC	lymphoid	59	48,XY,11q+,+19,22q-,+22q-(20/20)	RT-PCR
BC22	M	62	CML BC	myeloid	61	46,XY,t(20;22)(p13;q11)(8/20) 47,XY,t(20;22)(p13;q11),+der(22)t(20;22)(p13;q11)(5/20) 45,XY,del(4)(q31),add(6)(p21),der(8;17)(q10;q10),+i(8)(q10),+add(9)(p22),-13,-16,t(20;22)(p13;q11),der(22)t(20;22),inc(1/20) 44,X,-Y,add(6)(p21),der(8;17)(q10;q10),+i(8)(q10),add(9)(p22),-13,-16,t(20;22)(p13;q11),inc(1/20)	RT-PCR
BC23	M	28	CML BC	myeloid	36	74-87, ND, including add(6)(p21),der(8;17)(q10;q10),add(9)(p22),t(20;22)(p13;q11)(5/20)	FISH and RT-PCR
BC24	M	60	CML BC	myeloid	44	46,XY,t(9;22)(q34;q11)(18/20) 46,XY(2/20) 48,XY,+8,t(9;22)(q34;q11),+der(22)t(9;22)(q34;q11)(19/20)	FISH and RT-PCR
BC25	M	37	CML BC	myeloid	28	50,XY,+8,+8,t(9;22)(q34;q11),+21,+der(22)t(9;22)(q34;q11)(1/20)	FISH and RT-PCR
BC26	M	64	CML BC	myeloid	85	46,XY,t(9;22)(q34;q11)(12/20) 46,XY(8/20) 45,XY,add(5)(q15),der(9)t(9;22)(q34;q11),add(12)(p11),del(17)(p11),add(19)(q13),-21,der(22)add(22)(p11)t(9;22)(17/20)	FISH and RT-PCR

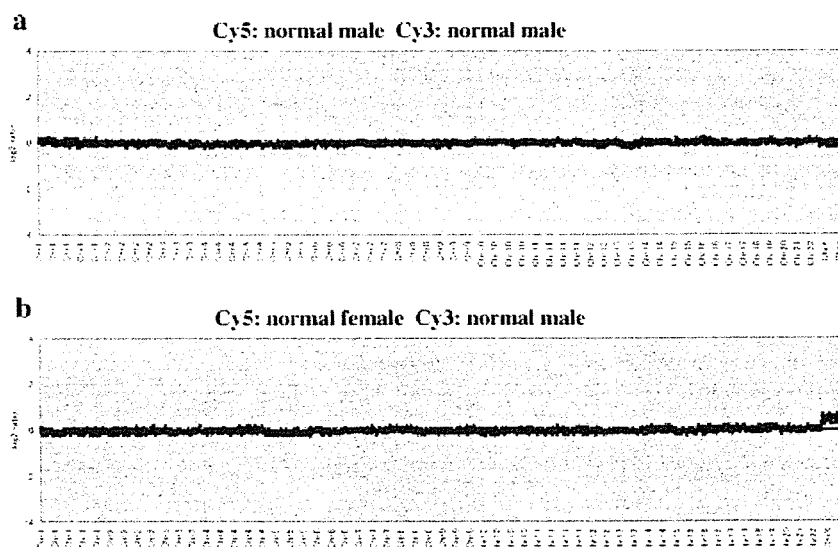
(Continued)

TABLE 1. Patient Characteristics, Cytogenetic Description of Their Karyotypes, and Presence of BCR/ABL Confirmed by FISH or RT-PCR (Continued)

Case No.	Sex	Age	Stage	Phenotype	Blast(%)	Karyotype	Methods of BCR/ABL detection
CP1	M	40	CML CP		0	45,X,Y,der(5)t(5:21)(q31;q11), der(9)t(9:22)(q34;q11), del(17)(p11).add(19)(q13), -21,der(22)add(22)(p11) t(9:22)(1/20)	
CP2	M	28	CML CP		0	48,X,Y,dup(3)(q21q27).add(4) (q21),der(5)t(5:21)(q31;q11), t(9:22)(q34;q11).add(13)(p11), del(17)(p11)+19,-21, +der(22)t(9:22)+mar(1/20)	
CP3	F	60	CML CP		0	48,X,Y,dup(3)(q21q27),-4, der(5)t(5:21)(q31;q11), t(9:22)(q34;q11).add(13)(p11), del(17)(p11)+19,-21, +der(22)t(9:22)+mar(1/20)	
CP4	M	62	CML CP		0	46,XX,t(9:22)(q34;q11)	
CP5	M	38	CML CP		5	46,XY,t(9:22)(q34;q11)	
CP6	M	35	CML CP		5	46,XY,t(9:22)(q34;q11)	
CP7	M	54	CML CP		0	46,XY,t(9:22)(q34;q11)	
CP8	F		CML CP		0	NA	
CP9	M		CML CP		0	46,XY,t(9:22)(q34;q11)	NS
CP10	M		CML CP		1	46,XY,t(9:22)(q34;q11)	NS
CP11	F	32	CML CP		0	46,XX,t(9:22)(q34;q11)	NS
CP12	F	59	CML CP		0	46,XX,t(9:22)(q34;q11)	NS
CP13	M	51	CML CP		0	46,XX,t(9:22)(q34;q11)	NS
CP14	F		CML CP		0	46,XX,t(9:22)(q34;q11)	NS
CP15	M	46	CML CP		0	46,XY,t(9:22)(q34;q11)	NS
CP16	M	58	CML CP		0	46,XY,t(9:22)(q34;q11)	NS
CP17	F	58	CML CP		0	46,XX,t(9:22)(q34;q11)	NS
CP18	F	74	CML CP		0	46,XX,t(9:22)(q34;q11)	NS
CP19	F	54	CML CP		0	46,XX,t(9:22)(q34;q11)	NS
CP20	M		CML CP		0.5	46,XY,t(9:22)(q34;q11)	NS
CP21	M	71	CML CP		0	46,XY,t(9:22)(q34;q11)(20/20)	NS
CP22	M	40	CML CP		0	46,XY,t(9:22)(q34;q11)(20/20)	FISH and RT-PCR
CP23	M	43	CML CP		1.5	46,XY,t(9:22)(q34;q11)(20/20)	FISH and RT-PCR
CP24	F	55	CML CP		2	46,XY,t(9:22)(q34;q11)(20/20)	NS
CP25	M	75	CML CP		0	46,XY,t(9:22)(q34;q11)	NS

ND: not determined; NA: information not available; NE: not examined; NS: not specified in clinical records; Ph chr: Philadelphia chromosome; chr: chromosome; RT-PCR: reverse-transcriptase-polymerase-chain-reaction; The t(20:22)(p13;q11) in case BC26 is a variant Ph translocation.

Figure 1. Representative array CGH results obtained from reference-versus-reference control hybridization. Clones are ordered from chromosomes 1 to 22, X, and Y and within each chromosome according to the UCSC mapping position (<http://genome.ucsc.edu/>; May 2004 draft). Each spot represents an average  $\log_2$  signal ratio for each BAC locus. (a) For all loci,  $\log_2$  ratios were within the thresholds  $-0.2$  and  $0.2$  in the male-versus-male control experiment. (b) Gain in chromosome X ( $0.435 \pm 0.124$ ) and loss in chromosome Y ( $-0.807 \pm 0.167$ ) were clearly visualized in the female-versus-male control experiment (Cy5 and Cy3, respectively).



applied to an array slide placed in a MAUI<sup>®</sup> Mixer AO Hybridization Chamber Lid (BioMicro Systems, Salt Lake City, UT) and incubated at 37°C for 60–66 h using a MAUI Hybridization System (BioMicro Systems). After hybridization, the slides were washed once in a solution of 50% formamide and 2× SSC for 15 min at 50°C and once in 2× SSC for 15 min at room temperature. Slides were rinsed briefly with 0.2× SSC and dried immediately by centrifugation.

#### Image Analysis and Processing

After hybridization, the arrays were scanned by an Affymetrix 428<sup>™</sup> Array Scanner (Affymetrix, Santa Clara, CA). The scanned image was analyzed by an ImaGene v4.2 (BioDiscovery, Inc., Marina Del Rey, CA) in order to extract Cy3 and Cy5 signals for each spot, and after local background signals were subtracted, test/reference  $\log_2$  ratios of the test and reference signals were calculated for all spots. The  $\log_2$  ratios were normalized so that the average  $\log_2$  ratio of all spots became zero. A spot was eliminated from the analysis if the signal intensity after the background subtraction in either Cy5 or Cy3 was less than  $-18$  decibels or the duplicated signals differed by more than 0.4 in the  $\log_2$  ratios. The average  $\log_2$  ratios of the two replicate spots were calculated for the remaining spots. An experiment was not adopted if less than 90% of all spots met the above-mentioned criteria or if the standard deviation (SD) of all spots was larger than 0.25. Thresholds for copy number gain and loss were defined as  $\log_2$  ratios of  $+2$  SD and  $-2$  SD, respectively. The reproducibility of the data was confirmed in two independent experiments for

each tumor sample. For two representative cases, the consistency of the CGH results was confirmed by dye-swap experiments, in which tumor and reference DNA were inversely labeled with Cy3 and Cy5, respectively.

#### FISH Analysis

Interphase FISH experiments were performed as previously described (Wang et al., 2003).

### RESULTS

#### Quality Test of BAC Array

Prior to the analysis of CML samples, control experiments were performed to evaluate the quality of the Human 1M array, in which DNA from normal individuals was used as a test sample. In the male-versus-male control hybridizations,  $\log_2$  ratios for all spots were within the thresholds of  $-0.2$  and  $0.2$  (Fig. 1a), whereas in the female-versus-male hybridizations, copy number gain of the whole chromosome X and copy number loss of the whole chromosome Y were detected successfully (Fig. 1b). In the latter experiments, the mean  $\log_2$  ratios of the clones on the X and Y chromosomes were  $0.435 \pm 0.124$  and  $-0.807 \pm 0.167$ , respectively, compared to the mean  $\log_2$  ratio of  $-0.008 \pm 0.083$  for all clones from autosomal chromosomes.

#### Higher Frequency of DNA Copy Number Changes in CML in BC and AP

A total of 55 CML samples in different stages were analyzed for copy number alterations by array CGH using Human 1M arrays. Table 2 lists the copy number alterations detected in individual

TABLE 2. Gains and Losses Detected by Array CGH

Case No.	Regions and clones that showed copy number gains	Regions and clones that showed copy number losses
AP1	3q26.2–q29 (RP11-91A17~RP11-233N20), 7p15.2–p14.3 (RP11-81F15~RP11-89N17)	22q13.2–q13.31 (RP11-81N15~RP11-66M5)
AP2	9p21.2 (RP11-81B19)-qter, Chromosome13, Chromosome19, Chromosome21, Chromosome22, <u>22q11.1–q11.22 and 9q34.13–qter</u> 22q13.1–q13.32 (RP11-4H24-RP11-133P21)	<b>8p23.1 (RP11-287P18)</b>
AP3	<b>5p15.1 (RP11-88L18, RP11-90B23), 19p13.2 (RP11-79F15)</b>	none
AP4	<b>8q21.2 (RP11-90G23)</b>	none
BC1	none	none
BC2	none	none
BC3	<b>4p15.33 (RP11-143I20), 5p15.1 (RP11-88L18) 8p12</b> (RP11-274F14-RP11-100B16), 9q, <b>19p13.2 (RP11-79F15),</b> <u>22q11.1–q11.22 and 9q34.13–qter</u>	<b>1q25.1 (RP11-177M16),</b> 5q23.1–q23.3 (RP11-47L19-RP11-89G4), 5q31.2–q32 (RP11-11514~RP11-88H2), 7q31.1–q31.33 (RP11-79G19~RP11-90C13), 8pter–p12 (RP11-91P13), 9p
BC4	<b>8p23.1 (RP11-287P18), 22q11.21 (RP11-278E23)</b>	none
BC5	<b>8p23.1 (RP11-287P18), 17p13.3 (RP11-582C6),</b> <b>19p13.2 (RP11-79F15)</b>	<b>17q21.31 (RP11-52N13)</b>
BC6	none	<b>5p15.1 (RP11-88L18)</b>
BC7	Chromosome8	none
BC8	none	none
BC9	none	<b>21q22.12 (RP11-17O20)</b>
BC10	<b>8p23.1 (RP11-287P18), 17p13.3 (RP11-582C6)</b>	none
BC11	none	none
BC12	<b>8p23.1 (RP11-287P18), 17p13.3 (RP11-582C6)</b>	<b>5p15.1 (RP11-88L18)</b>
BC13	none	Chromosomes 4 and 13
BC14	Chromosome8, <b>8q21.2 (RP11-90G23)</b>	none
BC15	<b>8p23.1 (RP11-287P18)</b>	none
BC16	Chromosome8*, <b>8p23.1 (RP11-287P18),</b> <u>Chromosome12*, 17p13.3 (RP11-582C6),</u> <u>22q11.1–q11.2 and 9q34.13–qter</u>	2q36.2–q37.3 (RP11-68H19~RP11-90E11*), <u>18pter–q11.2 (RP11-79F3)*</u>
BC17	none	<b>1q25.3 (RP11-196B7), 17q21.31</b> <b>(RP11-52N13)</b>
BC18	none	<b>1q25.3 (RP11-173E24),</b> <b>1q25.3–q31.1 (RP11-162L13)</b>
BC19	none	<b>5p15.1 (RP11-88L18),</b> 7p21.3–p11.2 (RP11-79O21~RP11-90N11)
BC20	none	<b>9q22.32 (RP11-223A21)</b>
BC21	<b>5p15.1 (RP11-88L18), Chromosome19*,</b> <u>22q11.1–q11.2 and 9q34.13–qter</u>	none
BC22	6p22.3 (RP11-43B4~RP11-288M24), 8p21.3 (RP11-89O4~RP11-274M9), 8p11.21 (RP11-282J24)-qter	8pter–p11.2 (RP11-284J3)
BC23	<b>5p15.1 (RP11-88L18)</b>	none
BC24	Chromosome8*, <b>17p13.3 (RP11-582C6),</b> <b>17q22 (RP11-143M4) 22q11.1–q11.2 and 9q34.13–qter</b>	<b>5p15.1 (RP11-88L18),</b> <b>7q11.21 (RP11-90C3)</b>
BC25	<b>5p15.1 (RP11-88L18), 19p13.2 (RP11-79F15)</b>	none
BC26	8q24.13–q24.21 (RP11-229L23-RP11-237F24), 19p13.2–p12 (RP11-84C17~RP11-91L5), <u>22q11.1–q11.2 and 9q34.13–qter</u>	none
CP1	<b>8p23.1 (RP11-287P18), 17p13.3 (RP11-582C6)</b>	<b>1q25.1 (RP11-177M16),</b> <b>1q25.3 (RP11-173E24),</b> <b>5p15.1 (RP11-88L18)</b>
CP2	<b>17q21.31 (RP11-52N13)</b>	<b>1q25.1 (RP11-177M16)</b>
CP3	<b>17p13.3 (RP11-582C6), 17q12(CTD-2019C10)</b>	<b>5p15.1 (RP11-88L18), 17q25.2</b> <b>(RP11-145C11)</b>

(Continued)

TABLE 2. Gains and Losses Detected by Array CGH (Continued)

Case No.	Regions and clones that showed copy number gains	Regions and clones that showed copy number losses
CP4	<b>5p15.1 (RP11-88L18),</b> <b>19p13.2 (RP11-79F15)</b>	<b>1q25.1 (RP11-177M16), 17q21.31</b> <b>(RP11-52N13)</b>
CP5	none	none
CP6	none	<b>5p15.1 (RP11-88L18)</b>
CP7	<b>19p13.2 (RP11-79F15)</b>	none
CP8	none	Chromosome3
CP9	none	none
CP10	none	none
CP11	none	none
CP12	<b>6q25.3-q26 (RP11-43B19)</b>	none
CP13	<b>8p23.1 (RP11-287P18),</b> <b>17p13.3 (RP11-582C6)</b>	none
CP14	<b>19p13.2 (RP11-79F15)</b>	none
CP15	8p23.2 (RP11-113B7~RP11-89I12), <b>8p23.1 (RP11-287P18),</b> <b>22q11.1-q11.2 and 9q34.13-qter</b>	none
CP16	<b>19p13.2 (RP11-79F15)</b>	<b>8q21.2 (RP11-90G23)</b>
CP17	none	none
CP18	<b>17p13.3 (RP11-582C6),</b> 17p11.2-qter	<b>17q12(CTD-2019C10)</b> 17pter-p12
CP19	none	none
CP20	<b>19p13.2 (RP11-79F15)</b>	<b>5p15.1 (RP11-88L18)</b>
CP21	<b>8p23.1 (RP11-287P18), 15q22.31 (RP11-50N10), 22q13.32</b> <b>(RP11-133P21)</b>	<b>1q25.1 (RP11-177M16)</b>
CP22	none	none
CP23	none	none
CP24	none	<b>5p15.1 (RP11-88L18, RP11-90B23),</b> <b>8q21.3 (RP11-91K2), 9q32 (RP11-95J4)</b>
CP25	none	none

**22q11.1-11.2 and 9q34.13-qter** corresponds to Philadelphia chromosome.

Gain of 17p11.2-qter together with loss of 17pter-p12 represents isochromosome 17q (i(17q)).

Copy number changes involving a single BAC are indicated in bold. Underlined are the regions (or BAC loci) whose copy number changes were confirmed by FISH.

cases, and Table 3 summarizes the number of cases showing each copy number alteration in different stages of CML. Array CGH successfully detected cryptic gains and losses that had been missed by conventional karyotyping analysis as well as large chromosomal changes that had been observed in prior conventional karyotyping analysis (Tables 2 and 3).

When analysis was confined to copy number alterations that involved at least two consecutive BAC clones, only 4 copy number alterations were detected in 25 patients in CP, whereas 38 copy number alterations were identified in 30 patients in AP/BC (Table 2). The frequency of DNA copy number alterations was significantly higher in AP/BC than in CP ( $P < 0.005$ ).

#### Large and Small Cryptic Changes Detected by High-Resolution Array CGH

In the current analysis, the most frequent alteration was gain of extra Ph chromosomes (6 cases in

AP/BC, 1 case in CP), which was inferred from gains of a distal part of 9q and a proximal part of 22q. Alterations of whole chromosomes, including gains of chromosomes 8 (4 cases in BC), 19 (2 cases in AP/BC), 13, 21, and 22 (1 case each in AP), and losses of chromosomes 3 (1 case in CP), 4, and 13 (1 case each in BC) were also observed (Tables 2 and 3). One CP patient (case CP18) displayed both gain of 17p11.2-qter and loss of 17pter-p12 material, suggesting the presence of an isochromosome 17q-i(17q)—which has repeatedly been reported in association with CML BC (Prigogina et al., 1978; Alimena et al., 1987; Fioretos et al., 1999; Melo et al., 2003), although the conventional karyotyping analysis had missed this abnormality.

Our array CGH analysis also uncovered cryptic changes that had not been reported in CML and therefore were novel regions implicated in the pathogenesis and progression of CML. Case BC3 was found to have a balanced t(9;22) translocation as the sole chromosomal abnormality in karyotyp-

TABLE 3. Summary of Copy Number Alterations Detected by Array CGH

	Stage	
	CP (n = 25)	AP + BC (n = 30)
<b>Gains</b>		
Unbalanced translocations or gains that were also detected by G-banding analysis		
Ph (22q11.1-q11.2 and 9q34.13-qter)	0	3
Chromosome 8	0	2
Chromosome 13	0	1
Chromosome 19	0	2
Chromosome 21	0	1
Chromosome 22	0	1
Gains in cases in which G-banding analysis was not done		
Chromosome 8	0	1
3q26.2-q29	0	1
7p15.2-p14.3	0	1
8p11.21-q24.3	0	1
Cryptic gains that were not detected by G-banding analysis (involving at least two consecutive BAC clones spotted on the array)		
Ph (22q11.1-q11.2 and 9q34.13-qter)	1	3
i(17q) (gain of 17p11.2-qter and loss of 17pter-p12)	1	0
Chromosome 8	0	1
6p22.3	0	1
8p12	0	1
8p21.3	0	1
8p23.2	1	0
8q24.13-q24.21	0	1
9p21.2-qter	0	1
9q	0	1
19p13.2-p12	0	1
22q13.1-q13.32	0	21
Total number	3	26
<b>Losses</b>		
Losses in cases in which G-banding analysis was not done		
Chromosome 3	1	0
Chromosome 4	0	1
Chromosome 13	0	1
7p21.3-p11.2	0	1
22q13.1-q13.31	0	1
Cryptic losses that were not detected by G-banding analysis (involving at least two consecutive BAC clones spotted on the array)		
2q36.2-q37.3	0	1
5q23.1-q23.3	0	1
5q31.2-q32	0	1
7q31.1-q31.33	0	1
8pter-p12	0	1
8pter-p11.2	0	1
9p	0	1
18pter-q11.2	0	1
Total number	1	12

ing analysis (Tables 1 and 2). However, in array CGH, multiple copy number alterations, including gains in 8p12 and 9q, and an extra Ph chromosome, and losses in 5q23.1-q23.3, 5q31.2-q32, 7q31.1-q31.33, 8pter-p12, and 9p were reproducibly detected in duplicate experiments (Table 2, Fig. 2a). Case BC16 had a karyotype showing 48,XY, t(3;21;18)(q21;q22;p11),+8, t(9;22)(q34;q11), +12 (Table 1), whereas array CGH also detected an extra Ph chromosome as well as losses in 2q36.2-q37.3 and 18pter-q11.2 (Table 2, Fig. 2b). Also, in case BC22, CGH analysis disclosed cryptic copy number gains in three consecutive BACs within a small 6p22.3 region spanning 505 kb (Table 2, Fig. 2c).

These array CGH results were confirmed by FISH analysis using affected BAC clones as probes when Carnoy samples were available (Table 2, Fig. 2b and c). For example, the sample from patient BC16 showed, consistent with trisomies 8 and 12, three signals from clones RP11-150N13, on chromosome 8 (with an average  $\log_2$  ratio of 0.449), and RP11-91I15, on chromosome 12 (with an average  $\log_2$  ratio of 0.474), whereas clones RP11-116M19, on chromosome 2 (with an average  $\log_2$  ratio of -0.538), and RP11-105C15, on chromosome 18 (with an average  $\log_2$  ratio of -0.701), produced only one signal, confirming the presence of an allelic deletion in these regions (Fig. 2b). In patient BC22, clones RP11-228M24, at 6p22.3 (with an average  $\log_2$  ratio of 1.158), showed multiple signals, in agreement with the copy number gain found in array CGH (Fig. 2c).

Copy number changes that involved only a single BAC locus (Table 4) were verified by FISH analysis for selected cases (Table 2 and Fig. 2d). In total, 75 single BAC copy number changes (SBCs) were identified in 24 BAC loci among 55 CML patients. Because 35 of the 75 SBCs, found in three BAC loci, were also identified in normal individuals (3 SBCs, at RP11-88L18, RP11-287P18, and RP11-586C6, in 10 healthy Japanese individuals; data not shown) and 37 SBCs in six BAC loci appeared as both copy number gains and losses depending on samples, suggesting that many of these are likely to represent polymorphisms known as large-scale copy number variations (LCVs; Iafrate et al., 2004; Sebat et al., 2004; Table 4). Indeed, 11 of the 24 BAC loci showing SBCs conformed to regions previously reported as LCVs (Table 4) (Iafrate et al., 2004; Sebat et al., 2004).

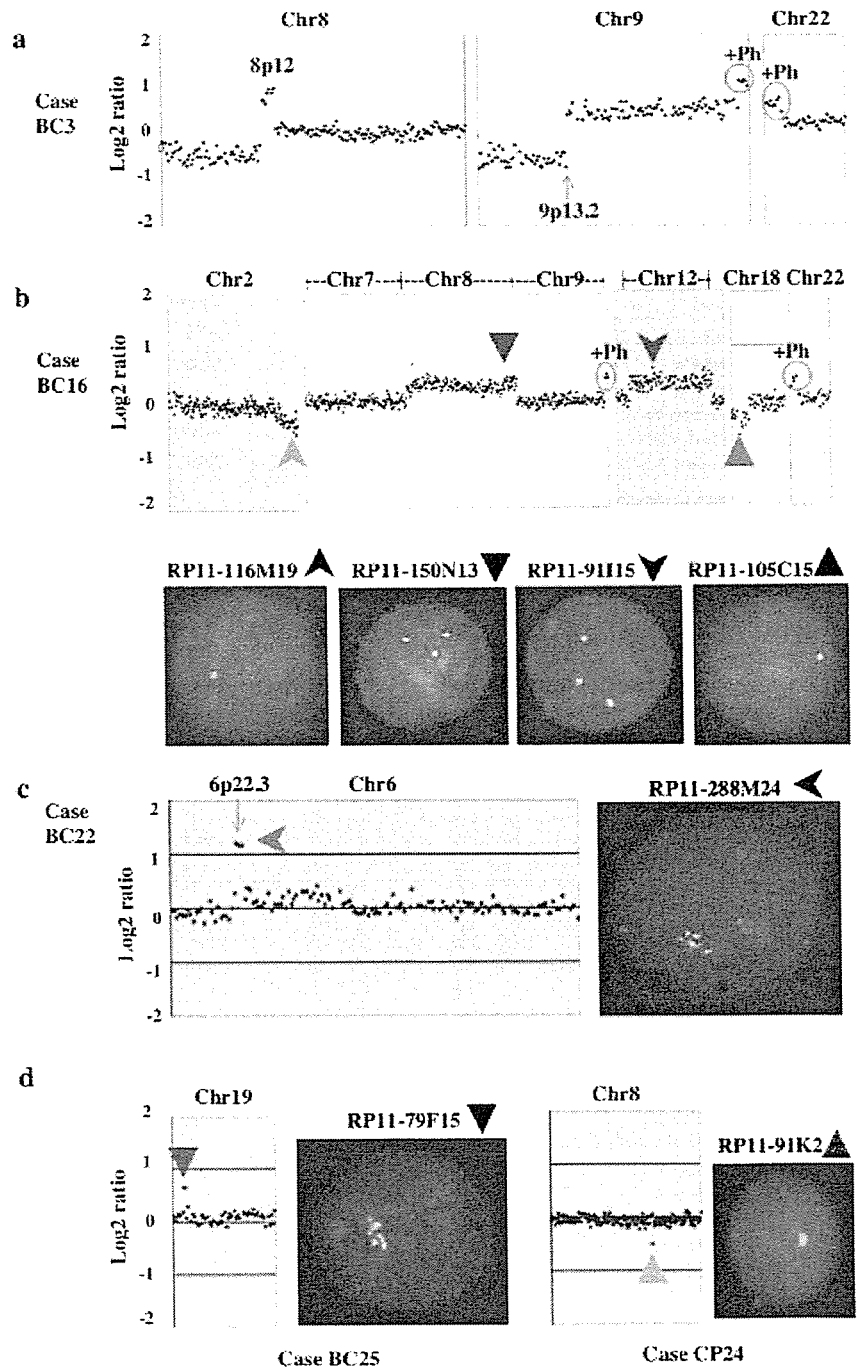


Figure 2. Gains and losses detected by array CGH and confirmed by FISH analysis. (a) Array CGH profile of case BC3, showing an extra Ph chromosome, gains in 8p12 and 9q and losses in 8pter–8p12 and 9p, not detected by karyotyping analysis; (b) Array CGH profile of case BC16, in which an extra Ph chromosome, gain in chromosome 8 with a higher-level of gain of the clone RP11-287P18, gain in chromosome 12, and losses in 2q36.2–2q37.3 and 18pter–18q11.2 were identified. Interphase FISH analysis of this case used the indicated biotin-labeled BAC clones as probes. Consistent with trisomies 8 and 12, clones RP11-150N13, on chromosome 8 (average log<sub>2</sub> ratio of 0.449), and RP11-91I15, on chromosome 12 (average log<sub>2</sub> ratio of 0.474), showed 3 signals, whereas clones RP11-116M19, on chromosome 2 (average log<sub>2</sub> ratio of –0.538), and RP11-105C15, on chromosome 18 (average log<sub>2</sub> ratio of –0.701), produced only one signal, confirming an allelic deletion in these regions. (c) Array CGH profile of case BC22, for which clone RP11-288M24, at chromosome 6p22.3 (average log<sub>2</sub> ratio of 1.158), showed multiple signals, confirming copy number gains in this region. (d) Array CGH profiles of cases BC25 and CP24, in which single BAC copy number changes were observed. Copy number gain (RP11-79F15) and loss (RP11-91K2) were verified by FISH analysis.

**Candidate Genes Implicated in Pathogenesis or Disease Progression of CML**

The regions showing gain or loss in DNA copy number or breakpoint regions of unbalanced chromosomal translocations could harbor one or more genes implicated in the pathogenesis of CML or disease progression to BC. Supplementary Table 2 lists the representative genes within these regions

identified in this study, not including the single BAC regions showing both gains and losses. Among previously reported cellular oncogenes or leukemia-related genes were *EVII* (3q26), *FGFR1* (8p12), and *MYC* (8q24), which were included in the regions showing copy number gains in 3q26.2–q29, 8p12, and 8q24.13–q24.21, respectively (Supplementary Table 2). The 505-kb region showing

TABLE 4. Copy Number Alterations Involving a Single BAC Locus

Locus	Stage	
	CP (n = 25)	AP + BC (n = 30)
<b>Gains</b>		
4p15.33 (RP11-143120) <sup>a</sup>	0	1
5p15.1 (RP11-88L18) <sup>a</sup>	1	5
5p15.1 (RP11-90B23)	0	1
6q25.3–q26 (RP11-43B19) <sup>a</sup>	1	0
8p23.1 (RP11-287P18) <sup>a</sup>	4	6
8q21.2 (RP11-90G23) <sup>a</sup>	0	2
15q22.31 (RP11-50N10)	1	0
17p13.3 (RP11-582C6) <sup>a</sup>	4	5
17q12 (CTD-2019C10)	1	0
17q21.31 (RP11-52N13)	1	0
17q22 (RP11-143M4)	0	1
19p13.2 (RP11-79F15) <sup>a</sup>	4	4
22q11.21 (RP11-278E23) <sup>a</sup>	0	1
22q13.32 (RP11-133P21)	1	0
<b>Losses</b>		
1q25.1 (RP11-177M16)	4	1
1q25.3 (RP11-196B7)	0	1
1q25.3 (RP11-173E24)	1	1
1q25.3–q31.1 (RP11-162L13)	0	1
5p15.1 (RP11-88L18) <sup>a</sup>	5	4
5p15.1 (RP11-90B23)	1	0
7q11.21 (RP11-90C3) <sup>a</sup>	0	1
8p23.1 (RP11-287P18) <sup>a</sup>	0	1
8q21.2 (RP11-90G23) <sup>a</sup>	1	0
8q21.3 (RP11-91K2) <sup>a</sup>	1	0
9q32 (RP11-95J4) <sup>a</sup>	1	0
9q22.32 (RP11-223A21)	0	1
17q12 (CTD-2019C10)	1	0
17q21.31 (RP11-52N13)	1	2
17q25.2 (RP11-145C11)	1	0
21q22.12 (RP11-17020)	0	1

Shaded areas point to the loci that showed both gains and losses in different samples.

<sup>a</sup>Regions previously reported to show large-scale copy number variations (LCVs).

copy number gain at the chromosome band 6p22.3 contained *OACT1* (*O*-acetyltransferase domain containing 1) and *E2F3* (*E2F* transcription factor 3), both known genes (Supplementary Table 2). It is not clear whether this region overlapped with the breakpoint region of the recurrent translocations  $t(6;19)(p22;q13)$  and  $t(6;9;22)(p22;q34;q11)$  in CML (Huret et al., 1989; Meza Espinoza et al., 2004; Yehuda et al., 1999), because the precise molecular breakpoints at 6p22 in these cases have not been characterized. The 346-kb region at 8p23.2 that showed copy number gain includes *CSMD1* (*CUB* and *sushi* multiple domains protein 1 precursor), the only transcriptome (Supplementary Table 2). Other abnormalities newly identified

in this study involved mostly large regions of 2q26.2–q37.3 (16.8 Mb), 5q23.1–q23.3 (10.6 Mb), 5q31.2–q32 (6.50 Mb), 7p15.2–p14.3 (6.14 Mb), 7p21.3–p11.2 (41.7 Mb), 7q31.1–q31.33 (17.9 Mb), 8p21.3 (2.18 Mb), and 19p13.2–p12 (12.1 Mb), which made it difficult to pinpoint the candidate target genes.

## DISCUSSION

In this article, we have shown genomewide detection of DNA copy number changes in a total of 55 CML patients at different stages using high-resolution array CGH. Using this technique, we delineated not only previously reported abnormalities, but also novel alterations involving narrow regions that may harbor only one or several candidate genes involved in the pathogenesis or disease progression of CML.

A number of cryptic copy number alterations that had been missed by karyotyping analysis were detected in array CGH analysis. Seven patients were found to have extra Ph chromosomes, which was the most frequent alteration in our series, although this alteration had not been detected by prior G-banding analysis in four of the seven patients (57%). In addition, more than 10 novel, cryptic copy number alterations were uncovered at a significantly higher frequency in patients in BC and AP, suggesting that these regions may contain genes relevant to the pathogenesis of CML, especially in progressive stages. Considering the wide variety of copy number alterations detected in AP/BC cases and that the majority of these abnormalities were observed in a single patient in our series, there might be a large heterogeneity in the molecular pathogenesis of CML AP/BC cases, and it may be possible that analysis of a larger number of patients could disclose novel recurrent molecular defects in CML. Alternatively, the genes included in the affected regions may also be deregulated by other mechanisms such as point mutations or epigenetic effects, which could not be detected by copy number analysis.

Many of the cryptic gains or losses affecting a single BAC locus are thought to represent copy number polymorphisms or LCVs rather than tumor-specific changes, and given their high frequency, it would be difficult to discriminate tumor-specific changes from LCVs. In our analysis, SBCs (or LCVs) seemed to be more frequently found in CML than in normal individuals using the same reference set (55 of 75 in CML vs. 3 of 10 in normal individuals,  $P = 0.021$ ). Although



recent reports suggested a possible association of some LCVs with the regions implicated in cancer development (Iafraite et al., 2004; Sebat et al., 2004), the precise role of the LCVs detected in the current analysis in the pathogenesis of CML is still unclear and should be addressed in future studies that would include a larger number of normal subjects.

Although array CGH analysis successfully unveiled cryptic genomic aberrations in CML, we should note that it also has limitations in that the tumor content of the samples clearly affected the sensitivity of detecting copy number changes in tumor components. According to our admixture experiments, in which mixed tumor and normal DNA were tested for detection of a trisomy, the threshold of tumor content for detection of trisomies in our array CGH was estimated to be more than 20%–40% tumor components (data not shown). Thus, the trisomy 8 in AP3 and the monosomy 21 in AP4 as revealed by G-banding analysis were not expected to be detected in array CGH analysis because abnormal metaphases were found in only 2 of 20 with AP3 and 5 of 20 with AP4 (Tables 1 and 2). On the other hand, array CGH failed to detect the loss of chromosome 21 found in 17 of 20 metaphases in G-banding analysis in BC26, which was most likely a result of karyotypic overrepresentation of one or more rapidly proliferating tumor subclones in G-banding analysis. Finally, the FISH Mapped Clones V1.3 collection distributed from BACPAC Resources Center, which we used for array construction, does not cover some regions of particular interest in CML pathogenesis. For example, deletions of the 5' region of the *ABL/BCR* junction on the der(9) chromosome, which is known to affect 10%–15% of the CML patients (Storlazzi et al., 2002), were missed in this study because our Human 1M arrays did not contain BAC clones including the *ABL* gene or the upstream *ASS* gene.

In conclusion, our array CGH analysis disclosed not only common chromosomal abnormalities, but also small, cryptic copy number alterations in CML genomes that were not detected by conventional analysis. It enabled a better description of genetic alterations in CML, which potentially could be applicable to molecular diagnostics and prediction of disease prognosis of this neoplastic disorder. The submicroscopic copy number alterations detected in this study might contribute to the identification of novel molecular targets implicated in the pathogenesis or disease progression of CML. Further studies with whole-genome tiling arrays

having much higher resolutions will help to detect precisely the genes involved in the disease progression of CML.

#### ACKNOWLEDGMENTS

We are grateful to the late professor Hisamaru Hirai (Department of Hematology and Oncology, University of Tokyo) for his encouragement in this work. We dedicate this paper to his memory. We also thank Ms. Yasuko Ogino and Mr. Kenjiro Masuda (Lab Company Limited, Tokyo, Japan) for their technical assistance.

#### REFERENCES

- Ahuja H, Bar-Eli M, Advani SH, Benchimol S, Cline MJ. 1989. Alterations in the p53 gene and the clonal evolution of the blast crisis of chronic myelocytic leukemia. *Proc Natl Acad Sci USA* 86:6783–6787.
- Albertson DG, Pinkel D. 2003. Genomic microarrays in human genetic disease and cancer. *Hum Mol Genet* 12 Spec No 2:R145–R152.
- Alimena G, De Cuia MR, Diverio D, Gastaldi R, Nanni M. 1987. The karyotype of blastic crisis. *Cancer Genet Cytogenet* 26:39–50.
- Beck Z, Kiss A, Toth FD, Szabo J, Bacsi A, Balogh E, Borbely A, Telek B, Kovacs E, Olah E, Rak K. 2000. Alterations of P53 and RB genes and the evolution of the accelerated phase of chronic myeloid leukemia. *Leuk Lymphoma* 38:587–597.
- Blick M, Romero P, Talpaz M, Kurzrock R, Shtalrid M, Andersson B, Trujillo J, Beran M, Gutterman J. 1987. Molecular characteristics of chronic myelogenous leukemia in blast crisis. *Cancer Genet Cytogenet* 27:349–356.
- Calabretta B, Perrotti D. 2004. The biology of CML blast crisis. *Blood* 103:4010–4022.
- Feinstein E, Cimino G, Gale RP, Alimena G, Berthier R, Kishi K, Goldman J, Zaccaria A, Berrebi A, Canaani E. 1991. p53 in chronic myelogenous leukemia in acute phase. *Proc Natl Acad Sci USA* 88:6293–6297.
- Fiegler H, Carr P, Douglas EJ, Burford DC, Hunt S, Scott CE, Smith J, Vetric D, Gorman P, Tomlinson JP, Carter NP. 2003. DNA microarrays for comparative genomic hybridization based on DOP-PCR amplification of BAC and PAC clones. *Genes Chromosomes Cancer* 36:361–374.
- Fioletos T, Strombeck B, Sandberg T, Johansson B, Billstrom R, Borg A, Nilsson PG, Van Den Berghe H, Hagemeijer A, Mitelman F, Hoglund M. 1999. Isochromosome 17q in blast crisis of chronic myeloid leukemia and in other hematologic malignancies is the result of clustered breakpoints in 17p11 and is not associated with coding TP53 mutations. *Blood* 94:225–232.
- Huret JL, Schoenwald M, Brizard A, Guilhot F, Vilmer E, Tanzer J. 1989. Chromosome 6p rearrangements appear to be secondary changes in various haematological malignancies. *Leuk Res* 13:819–824.
- Iafraite AJ, Feuk L, Rivera MN, Listewnik ML, Donahoe PK, Qi Y, Scherer SW, Lee C. 2004. Detection of large-scale variation in the human genome. *Nat Genet* 36:949–951.
- Kelman Z, Prokocimer M, Peller S, Kahn Y, Rechavi G, Manor Y, Cohen A, Rotter V. 1989. Rearrangements in the p53 gene in Philadelphia chromosome positive chronic myelogenous leukemia. *Blood* 74:2318–2324.
- LeMaistre A, Lee MS, Talpaz M, Kantarjian HM, Freireich EJ, Deisseroth AB, Trujillo JM, Stass SA. 1989. Ras oncogene mutations are rare late stage events in chronic myelogenous leukemia. *Blood* 73:889–891.
- Melo JV, Hughes TP, Apperley JF. 2003. Chronic myeloid leukemia. *Hematology (Am Soc Hematol Ed Prog)*:132–152.
- Meza Espinoza JP, Judith Picos Cardenas V, Gutierrez-Angulo M, Gonzalez Garcia JR. 2004. Secondary chromosomal changes in 34 Philadelphia-chromosome-positive chronic myelocytic leukemia patients from the Mexican West. *Cancer Genet Cytogenet* 148: 166–169.

- Mitani K, Ogawa S, Tanaka T, Miyoshi H, Kurokawa M, Mano H, Yazaki Y, Ohki M, Hirai H. 1994. Generation of the AML1-EVI-1 fusion gene in the t(3;21)(q26;q22) causes blastic crisis in chronic myelocytic leukemia. *Embo J* 13:504-510.
- Nakai H, Misawa S. 1995. Chromosome 17 abnormalities and inactivation of the p53 gene in chronic myeloid leukemia and their prognostic significance. *Leuk Lymphoma* 19:213-221.
- Nakai H, Misawa S, Taniwaki M, Horiike S, Takashima T, Seriu T, Nakagawa H, Fujii H, Shimazaki C, Maruo N and others. 1994. Prognostic significance of loss of a chromosome 17p and p53 gene mutations in blast crisis of chronic myelogenous leukaemia. *Br J Haematol* 87:425-427.
- Nakai H, Misawa S, Toguchida J, Yandell DW, Ishizaki K. 1992. Frequent p53 gene mutations in blast crisis of chronic myelogenous leukemia, especially in myeloid crisis harboring loss of a chromosome 17p. *Cancer Res* 52:6588-6593.
- Nakamura T, Largaespada DA, Lee MP, Johnson LA, Ohyashiki K, Toyama K, Chen SJ, Willman CL, Chen IM, Feinberg AP, Copeland NG, Jenkins NA, Shaughnessy JD Jr. 1996. Fusion of the nucleoporin gene NUP98 to HOXA9 by the chromosome translocation t(7;11)(p15;p15) in human myeloid leukaemia. *Nat Genet* 12:154-158.
- Pinkel D, Segraves R, Sudar D, Clark S, Poole I, Kowbel D, Collins C, Kuo WL, Chen C, Zhai Y, Dairkee SH, Ljung BM, Gray JW, Albertson DG. 1998. High resolution analysis of DNA copy number variation using comparative genomic hybridization to microarrays. *Nat Genet* 20:207-211.
- Prigogina EL, Fleischman EW, Volkova MA, Frenkel MA. 1978. Chromosome abnormalities and clinical and morphologic manifestations of chronic myeloid leukemia. *Hum Genet* 41:143-156.
- Rowley JD. 1973. Letter: A new consistent chromosomal abnormality in chronic myelogenous leukaemia identified by quinacrine fluorescence and Giemsa staining. *Nature* 243:290-293.
- Sebat J, Lakshmi B, Troge J, Alexander J, Young J, Lundin P, Maner S, Massa H, Walker M, Chi M, Navin N, Lucito R, Healy J, Hicks J, Ye K, Reiner A, Gilliam TC, Trask B, Patterson N, Zetterberg A, Wigler M. Large-scale copy number polymorphism in the human genome. *Science* 305:525-528.
- Sill H, Goldman JM, Cross NC. 1995. Homozygous deletions of the p16 tumor-suppressor gene are associated with lymphoid transformation of chronic myeloid leukemia. *Blood* 85:2013-2016.
- Wang L, Ogawa S, Hangaishi A, Qiao Y, Hosoya N, Nanya Y, Ohyashiki K, Mizoguchi H, Hirai H. 2003. Molecular characterization of the recurrent unbalanced translocation der(1;7)(q10;p10). *Blood* 102:2597-2604.
- Yehuda O, Abeliovich D, Ben-Neriah S, Sverdlin I, Cohen R, Varadi G, Orr R, Ashkenazi YJ, Heyd J, Lugassy G, Ben Yehuda D. 1999. Clinical implications of fluorescence in situ hybridization analysis in 13 chronic myeloid leukemia cases: Ph-negative and variant Ph-positive. *Cancer Genet Cytogenet* 114:100-107.